Subject-Independent Estimation of Continuous Movements Using CNN-LSTM for a Home-Based Upper Limb Rehabilitation System

He Li, *Graduate Student Member, IEEE*, Shuxiang Guo, *Fellow, IEEE*, Dongdong Bu, *Member, IEEE*, Hanze Wang, *Student Member, IEEE*, and Masahiko Kawanishi

***Abstract*—Exoskeleton-assisted home-based rehabilitation plays a vital role in the upper limb rehabilitation of stroke patients in early stage. The surface electromyography (sEMG)-based control can facilitate friendly interactions between individuals and rehabilitation exoskeletons. The exoskeleton can also meet the requirements of home-based rehabilitation, including affordability, portability, safety, and active participation. Although various systems have been proposed to enhance upper limb training, few studies have addressed the inter-subject variability of sEMG signals, which limits the generalization capability of the intention estimation model. In this letter, a subject-independent continuous motion estimation method combining convolutional neural networks (CNN) and long and short-term memory (LSTM) is proposed and applied to a home-based bilateral training system. The sEMG-driven CNN-LSTM model builds the relationship between sEMG signals and continuous movements. To verify the effectiveness of the CNN-LSTM model in achieving subject-independent estimation, the offline estimation under the backpropagation neural network, CNN, and CNN-LSTM are compared. Moreover, the online intention estimation and the real-time control are performed, and the estimation angle error and time delay are controlled at approximately 10° and 300 ms, proving the feasibility of the subject-independent estimation method and its availability in the upper-limb rehabilitation system.**

Manuscript received 22 February 2023; accepted 24 July 2023. Date of publication 9 August 2023; date of current version 28 August 2023. This letter was recommended for publication by Associate Editor D. Paez-Granados and Editor A. Peer upon evaluation of the reviewers' comments. This work was supported in part by the National Natural Science Foundation of China under Grant 61703305, in part by the National High-Tech Research and Development Program through 863 Program of China under Grant 2015AA043202, and in part by SPS KAKENHI under Grant 15K2120. *(Corresponding author: Shuxiang Guo.)*

This work involved human subjects or animals in its research. Approval of all ethical and experimental procedures and protocols was granted by Institutional Review Board (IRB) of the Faculty of Engineering and Design at Kagawa University under Application No. 01-011, and performed in line with the Declaration of Helsinki.

He Li, Dongdong Bu, and Hanze Wang are with the School of Life Science, Beijing Institute of Technology, Beijing 100081, China, and also with the Key Laboratory of Convergence Biomedical Engineering System and Healthcare Technology, The Ministry of Industry and Information Technology, Beijing Institute of Technology, Beijing 100081, China (e-mail: lihe@bit.edu.cn; budongdong@bit.edu.cn; wanghanze@bit.edu.cn).

Shuxiang Guo is with the Intelligent of Mechanical System Engineering Department, Kagawa University, Takamatsu 761-0793, Japan, and also with the Key Laboratory of Convergence Medical Engineering System and Healthcare Technology, Ministry of Industry and Information Technology, Beijing Institute of Technology, Beijing 100081, China (e-mail: guo.shuxiang@kagawa-u.ac.jp).

Masahiko Kawanishi is with the Department of Neurological Surgery, Faculty of Medicine, Kagawa University, Takamatsu 761-0793, Japan (e-mail: mk@kms.ac.jp).

Digital Object Identifier 10.1109/LRA.2023.3303701

***Index Terms*—Intention recognition, rehabilitation robotics, deep learning methods, model learning for control, motion control.**

I. Introduction

HEMIPARESIS of the upper limb is a common sequela of stroke, which occurs in about 85% of patients in the early stage. Particularly, rehabilitation training is most effective in the first three months after the onset of stroke [1]. Therefore, rehabilitation training in the early stage of stroke is vital. But the upper limb rehabilitation training for hemiparetic patients requires long-term training under the guidance of experts [2], which is challenging. Long-term professional rehabilitation training requires families to bear high costs while putting forward further requirements for the workload of physiotherapists. The inability to bear high costs and the lack of medical resources eventually lead to the interruption of training, resulting in the inability to ensure timely and effective treatment and missing the optimal recovery period.

In recent years, robotic exoskeleton-assisted devices have been developed to improve the functional movements of hemiplegic patients, which can provide a quantitative and objective evaluation for the rehabilitation process [3]. Furthermore, exoskeleton-assisted rehabilitation training can improve the motivation of hemiparesis patients to participate in rehabilitation more effectively than traditional training. Bilateral rehabilitation training protocol is considered an effective strategy for the rehabilitation of hemiplegic patients [4], in which the intact limb drives the affected limb to carry out synchronous motions. Intention recognition of intact side movement can be divided into indirect recognition based on inertial and force sensors, and direct recognition based on physiological signals. As a physiological signal that is easy to collect, surface electromyography (sEMG) signals have been widely used in exoskeleton devices. The sEMG-driven motion control can be an optimal way to achieve harmonious interaction between users and rehabilitation robots [5], [6], [7].

Many different sEMG-based rehabilitation systems have been developed recently [8], [9], [10], [11], [12], [13], [14]. Several researchers have estimated muscular torques (or motion angles) from sEMG using a musculoskeletal model. These approaches have been applied to the upper limb [8], [9] and lower limb [10], [11] exoskeletons. Buongiorno et al. [8] proposed a linear optimization method to adapt a simplified sEMG-based neuromusculoskeletal model to a specific user. Liu et al. [9] presented a bilateral rehabilitation system that enables real-time stiffness adjustment through sEMG-based stiffness

control. As an alternative to the musculoskeletal model-based method, some research groups have proposed using machine learning to establish the relationship between sEMG and muscular torque (or motion angles) [15], [16], [17]. Yang et al. [15] proposed an sEMG-based bilateral training system in which offline and online experiments were designed to verify the rehabilitation training system. Xiao et al. [16] realized the estimation of continuous angles from sEMG by utilizing multiple time-delayed features and random forests. Li et al. [17] combined multisource domain adaptation with a shallow neural network to continuously estimate elbow joint movements.

However, there are several limitations to the above systems. First, the high cost of traditional sEMG acquisition devices, the tedious steps of electrode placement, and the inconvenience of donning and doffing the sEMG sensor make them unsuitable for home-based rehabilitation [18]. The second reason has to do with the inter-subject variability of sEMG. Considering the inter-subject variability, Yang et al. [15], Li et al. [17], Trigili et al. [19], and Guo et al. [20] attempted various methods to mitigate or eliminate it. Yang et al. [15] utilized common time-domain and frequency-domain features to construct subject-independent models. Trigili et al. [19] selected user-independent features with the aid of the information theory tool. Li et al. [17] extracted user-invariant features by MDA and subsequently achieved the inter-subject independent continuous estimation of elbow joint movements. However, these approaches have their limitations. Yang et al. [15] and Trigili et al. [19] relied solely on traditional time-domain and frequency-domain features, which have not significantly addressed the issue of inter-subject variability. The methods of Guo et al. [20] and Li et al. [17] are offline but cannot be applied to real-time control. Therefore, the development of an sEMG-driven upper limb exoskeleton rehabilitation system that is affordable, portable, and subject-independent is an urgent task. This system can be applied in home-based rehabilitation for patients with upper limb hemiplegia, through which motor function can be improved.

This study introduces an sEMG-driven bilateral training system using a gear-driven powered upper limb exoskeleton device (GP-ULED) for upper limb rehabilitation. The rehabilitation system can estimate the continuous movements of the intact side by sEMG and then provide the symmetrical movements in sync to drive the affected side in real time by GP-ULED. For the subject-independent prediction of elbow joint angles, a CNN-LSTM which can extract the spatial and temporal features is built using sEMG images in the offline stage. Then it can be applied to online estimation and real-time myoelectric control. The experiments on 10 healthy subjects verify the feasibility of the proposed system. Results, including the offline result comparison and real-time control performance, are presented and discussed, indicating that the proposed rehabilitation system has the potential to be applied in upper limb training for stroke patients. To sum up, the main contributions of this letter are as follows:

1) Considering the inter-subject variability of sEMG, CNN-LSTM is adopted to extract transferable features among different subjects for subject-independent estimation of continuous movements.
2) Based on the CNN-LSTM model, online intention estimation and real-time control are implemented for the home-based upper limb rehabilitation system.

The rest of this letter is organized as follows: Section II describes the involved methods in detail, including the exoskeleton structure and control hardware, the sEMG measurement device, the embedded control system, the offline data acquisition and preprocessing of sEMG, the data set construction, the CNN-LSTM modeling and angle estimation, and evaluation criteria, in turn. The results of the offline and online experiments are shown in Section III. Section IV presents the discussion. Section V serves as the conclusion of this letter.

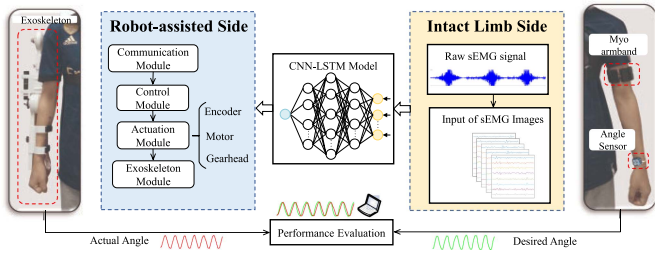

Fig. 1. Overview of subject-independent estimation of continuous movements using CNN-LSTM for home-based bilateral upper limb rehabilitation system.

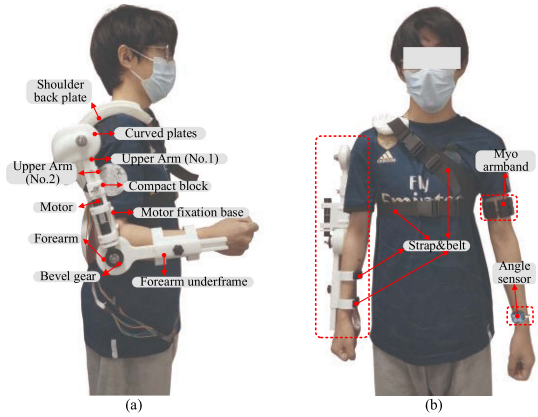

Fig. 2. Upper limb exoskeleton device. (a) Lateral view (b) front view.

II. Methods

Fig. 1 presents the overall framework of the proposed home-based bilateral rehabilitation system for upper limb training. Bilateral training is a rehabilitation strategy in which the intact limb drives the affected limb to carry out symmetrical movements in sync, assisted by the robot. In the proposed system, a gear-driven portable exoskeleton is utilized as the hardware platform to achieve sEMG-based real-time control for robot-assisted rehabilitation training. The sEMG-driven subject-independent estimation of continuous movements is realized through a CNN-LSTM model with sEMG images as input.

A. Exoskeleton Structure and Control Hardware

Overview of the GP-ULED is depicted in Fig. 2. It has two passive degrees of freedom (DoFs) at the shoulder, which are shoulder adduction/abduction and shoulder flexion/extension, and one active DoF at the elbow, which is elbow flexion/extension (passive DoF refers to the rotation resulting from human movements, active DoF refers to the rotation resulting from the gear-driven mechanism). The length of the upper arm of the exoskeleton and

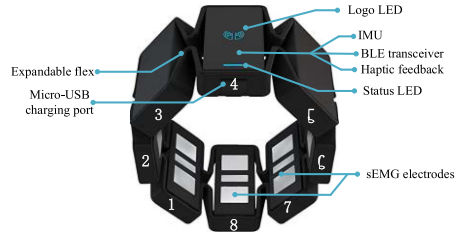

Fig. 3. Myo armband from thalmic labs.

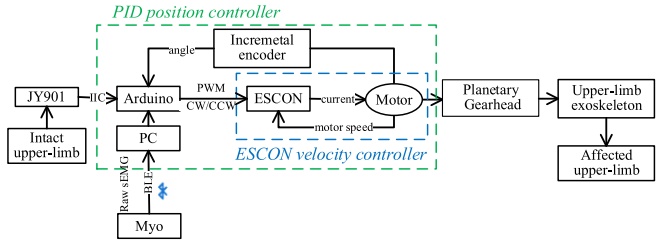

Fig. 4. Overall design of the embedded system of the upper limb rehabilitation exoskeleton.

the position of the forearm underframe can be adjusted. To reduce structural weight and cost while maintaining accuracy, the primary exoskeletal frames are 3D printed using curable resin. It is lightweight and allows for small physical configurations, providing high versatility to accommodate different users. The total weight of GP-ULED is only 1.35 kg, which is shared by two fabric straps (as shown in Fig. 2(b), one around the waist and one as a shoulder harness attached to the torso).

A gear-driven elbow exoskeleton (shown in Fig. 2(a)) powered by a brushless motor (EC22, Maxon, Switzerland) serves as the hardware platform for testing the sEMG-based subject-independent estimation of continuous movements. The brushless motor, coupled with a gearbox (Maxon Planetary Gearhead GP 22 HP) and a quadrature optical encoder (MR M-512) is utilized to control the rotation angle of the elbow joint with the help of gear. The brushless motor is placed along the upper arm, which reduces the burden on the forearm and minimizes obstacles. The motor is controlled by a matched motor controller (ESCON 50/5, Maxon). The two bevel gears are made of 45 steel, and their gear ratio is 1:2. In addition, the backlash between the two gears can be reduced by adjusting their positions through the oblong fixation base of the motor.

B. sEMG Measurement Device

Intention detection based on sEMG is the gold standard for portable devices [21]. In this study, the Myo armband is used for sEMG acquisition. The Myo armband from Thalmic Labs (as shown in Fig. 2(b)) utilizes eight dry sEMG sensors to measure and record electrical impulses from the user's muscles. The sampling frequency of the Myo armband is 200 Hz. Bluetooth Low Energy (BLE) is its communication mode, which simplifies wireless connectivity with other devices. Compared with other sEMG data acquisition devices, the Myo armband is preferred for its advantages of low cost and ease of use et al. It can be easily donned and taken off without the therapist and is user-friendly [22] due to the expandable flex that allows for adjustments to fit any forearm size (as shown in Fig. 3), and it also has been applied in rehabilitation [23], [24], [25]. Meanwhile, a compact inertial measurement unit (IMU, type: JY901, WIT) is attached to the intact limb to record the target angles. IIC is used to communicate between the JY901 and the microcontroller because it can transmit data more reliably than serial ports.

C. Embedded Control System

The control architecture of the GP-ULED is divided into two modules: high-level and low-level control. The high-level control is based on an sEMG-driven neural network (CNN-LSTM) model implemented in MATLAB (2022b, MathWorks). The low-level control of the exoskeleton and data logging are executed through an Arduino (Mega 2560), which collects angle data from the IMU and the PC, respectively. The Arduino communicates with MATLAB at a baud rate of 115200 bps. The real-time low-level control is based on an outer position loop and an inner velocity loop. The servo motor's Hall sensor provides information to the servo driver for controlling the motor's speed. The servo driver uses feedback information to adjust and achieve closed-loop control of the servo motor. In the outer position loop of the bilateral rehabilitation, the control system utilizes the deviation between the angles of the intact side and the angles of the exoskeleton motor for proportional-integral-differential closed-loop control, in which the resulting position error is transformed into a desired angular velocity. Fig. 4 presents the overall design of the embedded system of GP-ULED.

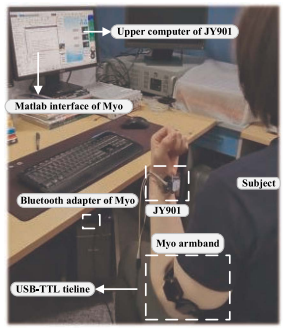

Fig. 5. Schematic diagram of the offline data acquisition.

D. Data Acquisition and Preprocessing of sEMG

The study involved ten subjects (labeled as Subject 1- Subject 10): five females and five males, with an average age of 25.4 ± 1.38 years (mean ± standard deviation). All participants are free from skeletal and neurological diseases, and can achieve a normal range of motion for the elbow joint. All participants provided explicit written consent to participate in this research.

The diagram for offline data acquisition is presented in Fig. 5. The sEMG data is collected at a frequency of 200 Hz using the Myo armband. Since each data acquisition lasted 1 minute, the number of sampling points per subject in each acquisition is 12000, and each subject repeats the experiment 5 times. The IMU with a sampling frequency of 20 Hz is attached to the forearm to record the motion angle of the elbow joint, which is taken as the reference signal to compare with the estimation results. After completing offline data acquisition, it is necessary to preprocess the collected sEMG signal because the raw sEMG is weak and sensitive to noise. The high-pass filter at 20 Hz eliminates DC offsets and low-frequency noises

TABLE I
PREDICTION TIME FOR A SINGLE-POINT SEMG INPUT (MS)

	1	2	3	4	5	Ave
BPNN	14.966	15.137	16.512	16.455	15.074	15.629
CNN	9.462	10.468	7.311	8.730	8.854	8.965
CNN-LSTM	14.408	12.198	11.838	11.897	12.152	12.499

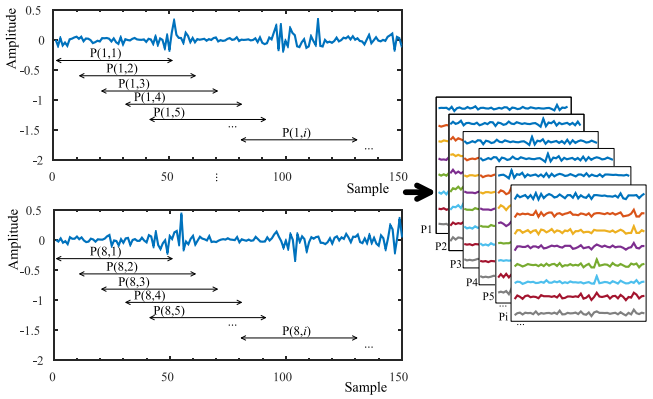

Fig. 6. Conversion of sEMG signals to sEMG images by the method of sliding window. P(a,b) represents a segment of sEMG signal from channel b at time a. Pa represents the sEMG signals from 8 channels.

that could potentially interfere with the sEMG signal. The Myo armband is embedded with a 50 Hz notch filter that effectively eliminates power-line interference (50 Hz). The Euler angles outputted by the IMU are filtered by the embedded dynamic Kalman filter algorithm embedded in IMU, so there is no need for any additional filtering processing.

E. Data Set Construction

Since sEMG is a highly non-stationary signal, the sampled signals should be divided into short time windows to ensure signal stability. The segment length should be large enough to avoid degradation of regression performance. However, the segment size should also be small enough to meet the requirements for real-time control, which means the sEMG signal should be less than 300 ms, which includes the window length and processing time for generating the control command. To certain the time of generating control commands, the single-point sEMG signal is used as the input of CNN-LSTM to record the prediction time. Table I records the prediction time. The sEMG signals in each channel are segmented using a sliding window with a length of 250 ms (50 sampling points), which is incremented by 50 ms (10 sampling points). Based on the above, the number of sliding windows for each subject in each data acquisition is 1196 (12000-50+10)/10 = 1196. Since the ratio of the sampling frequency of sEMG and IMU is 10:1, the IMU angle signal is also segmented using a sliding window with a length of 25 ms and an increment of 5 ms.

In the backpropagation neural network (BPNN), three time-domain features (integrated absolute value, mean absolute value, and root mean square) of each channel are extracted to construct a 24-dimensional feature vector. For the CNN and CNN-LSTM, the sEMG signals from 8 channels of the Myo armband are transformed into sEMG images with a size of 50 × 8. Fig. 6 illustrates the conversion of sEMG signals to sEMG images using the sliding window method.

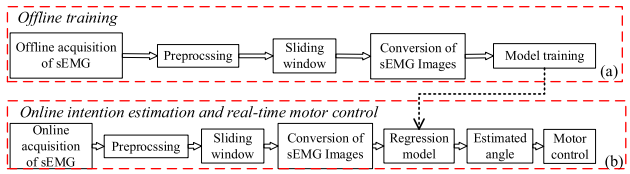

Fig. 7. Flow diagram of the training and estimation. (a) Offline training (b) online estimation.

F. CNN-LSTM Modeling and Angle Estimation

Unlike traditional shallow neural networks, deep neural networks emphasize the importance of feature learning. That is, the feature representation of samples in the original space is transformed into a new feature space by layer-by-layer feature transformation so that the prediction can be more straightforward. The sEMG features automatically extracted and constructed through the network layer are complete and more comprehensive than a single feature or a combination of features designed by artificial rules. Principal component analysis and other factorization methods rely on features designed by artificial rules. These methods only consider the irrelevance among different features without considering the transferring of features. Recent studies [26], [27] have shown that deep neural networks are capable of learning transferable features, producing groundbreaking results on domain adaptation datasets. The sEMG signals exhibit high inter-subject variability, and deep neural networks provide an effective approach to extracting transferable features. Based on the above, CNN is used for sEMG-based angle estimation.

In addition to the inherent inter-subject variability, sEMG signals are essentially sequential in nature. Therefore, using a recurrent neural network (RNN) for regression problems is valuable. Compared with RNN, LSTM addresses the issue of gradient disappearance and gradient explosion during long sequence training, resulting in better performance for longer sequences. Although LSTM is effective in processing time-sequential data, it cannot portray the spatial features of time-sequential data, such as images. Since sEMG signals are both time and space-related, LSTM in combination with convolution operation to capture spatial features is more effective for image feature extraction, that is, CNN-LSTM [28]. Thus, CNN-LSTM is chosen to predict the continuous flexion-extension motions of the upper limb elbow.

The sEMG-based bilateral training consisted of two stages. The subjects perform continuous flexion-extension motions. Then the input data of CNN-LSTM can be obtained through preprocessing, sliding window, and conversation of sEMG images. Offline training and estimation are used to verify the validity of the CNN-LSTM model for subject-independent motion recognition. It also provides a model for online estimation and real-time control. Only the model with good offline prediction performance can be deployed in the online estimation and real-time bilateral control phases. That is, the online intention estimation and real-time motor control are based on the model trained in the offline phase. The details of these two phases are recorded in Fig. 7.

1) Offline Training and Estimation: The offline training and estimation (as shown in Fig. 7(a)) are based on the sEMG data collected offline. In this study, the CNN-LSTM model consists of

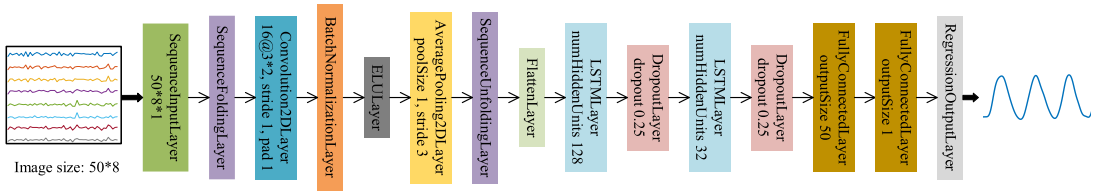

Fig. 8. Schematic of the CNN-LSTM used on sEMG signals.

15 layers: one convolutional layer, two LSTM layers, two fully-connected layers, and a regression output layer. The specific neural network model is depicted in Fig. 8. The sEMG images obtained by the sliding window method serve as the input of CNN-LSTM, and the estimated angle is the output of CNN-LSTM. The size of the input layer for the sequence depends on the size of the sEMG images, and the number of output layer neurons depends on the number of output variables. Through CNN-LSTM, the estimated angle signal of elbow movements can be calculated. To be further applied to sEMG-controlled human-robot interfaces (HRIs), the sliding window method is adopted to filter the angle signal.

2) Online Angle Estimation and Real-Time Control of GP-ULDE: The online angle estimation and real-time control of GP-ULDE (as shown in Fig. 7(b)) are reliant on the CNN-LSTM model that has been trained. The GP-ULDE is worn on the affected side, as shown in Fig. 2. The JY-901 captures the angle data of the intact side. The participants perform elbow joint movements according to the same rules as offline data acquisition. In this stage, sEMG data acquisition, preprocessing, data set construction, angle estimation, and GP-ULDE control are all performed in real time. The participants perform the pre-defined sequence of movements consistent with the offline phase through the intact upper extremity. The estimation angles can be calculated in real time through the CNN-LSTM model, and the whole prediction process is realized in Matlab, which facilitates high-level control. The estimation results obtained in real-time are then transmitted to Arduino via serial communication, which implements the low-level control. Finally, real-time control of GP-ULDE can be achieved based on the high-level and low-level control loops.

G. Evaluation Criteria

For quantitative assessment, the evaluation criteria of Root Mean Square Error (RMSE), Mean Absolute Error (MAE), Sum of Squares Error (SSE), and Correlation Coefficient (R^2) are adopted. RMSE is the square root of MSE, which is more intuitive in terms of magnitude. MAE is the average error between the estimated values and the target values, as demonstrated in (1). MAE is utilized to calculate the mean absolute error between the estimated values and the true values, as shown in (2). SSE calculates the sum of the squares of the errors between the estimated values and the target values at each corresponding point, as shown in (3). R^2 is used to measure the fitting effect of the regression model, as shown in (4), and the closer to 1, the better the fitting effect.

$$RMSE = \sqrt{\frac{1}{N}\sum_{i=1}^{N}(y_i - x_i)^2} \tag{1}$$

TABLE II
PARAMETERS OF BPNN, CNN, AND CNN-LSTM MODEL

	Average time (ms)	Average size (MB)	Input dimension	Output dimension
BPNN	15.629	7.85	[24 1]	1
CNN	8.965	2.78	[50 8]	1
CNN-LSTM	12.499	1.80	[50 8]	1

$$MAE = \frac{1}{N}\sum_{i=1}^{N}(y_i - x_i) \tag{2}$$

$$SSE = \sum_{i=1}^{N}(y_i - x_i)^2 \tag{3}$$

$$R^2 = 1 - \sum_{i=1}^{N}(x_i - y_i)^2 / \sum_{i=1}^{N}(x_i - \bar{y})^2 \tag{4}$$

Where x_i represents the actual value at the ith data point, y_i represents the estimated value at the ith data point, $\bar{x}$ is the average of all true values, $\bar{y}$ is the average of the estimated values, and N is the total number of data points.

III. RESULTS

This section presents the results of the CNN-LSTM model in both offline and real-time scenarios. The offline estimation results of CNN-LSTM, BPNN, and CNN are compared using various evaluation metrics for quantitative assessment. The involved software is implemented on a 64-bit Windows machine (Intel(R) Core (TM) i7-4790 CPU @ 3.60GHz 3.60 GHz). The neural network is run in MATLAB, while the real-time control of the exoskeleton is carried out using Arduino. In addition, the raw sEMG data is transmitted to MATLAB via BLE.

1) Offline Training and Estimation: For all subjects (1–10), the data of the first seven (1–7) are used for modeling, while the last three (8–10) serve as the additional test sets. And the sEMG segments used for modeling are 41860 ($7\times5\times1196 = 41860$). During the modeling of BPNN, the proportion of the training set, test set, and validation set is 70%:15%:15%. During the modeling of CNN and CNN-LSTM, the ratio of the training set to the validation set is 70%:30%. The parameters of BPNN, CNN, and CNN-LSTM are listed in Table II. Fig. 9 shows the offline angle estimation under BPNN, CNN, and CNN-LSTM. Fig. 9(a)–(c) show the offline angle prediction results of participants 8–10, respectively. The angles obtained by IMU, BPNN, CNN, and CNN-LSTM are plotted in each figure. Table III records the quantitative evaluation of offline angle estimation under BPNN, CNN, and CNN-LSTM. The comparison of prediction effects shown in Fig. 9(a)–(c) can reflect the inter-subject variability of sEMG. For Subject 8, the prediction performance of three

TABLE III
QUANTITATIVE EVALUATION OF OFFLINE ANGLE ESTIMATION UNDER BPNN, CNN, AND CNN-LSTM

	Test1 (subject 8)			Test2 (subject 9)			Test3 (subject 10)		
	BPNN	**CNN**	**CNN-LSTM**	**BPNN**	**CNN**	**CNN-LSTM**	**BPNN**	**CNN**	**CNN-LSTM**
RMSE	29.8445	17.4399	**15.1952**	18.2303	17.1420	**15.3746**	15.8554	17.1928	**15.2089**
MAE	22.7426	13.7905	**12.8540**	14.4615	14.6854	**13.0131**	12.1731	13.6232	**11.3080**
SSE	1.0653 e+06	3.6376 e+05	**2.7615 e+05**	3.9748 e+05	3.5144 e+05	**2.8271 e+05**	3.0067 e+05	3.5353 e+05	**2.7665 e+05**
R^2	0.7106	0.9012	**0.9250**	0.8979	0.9097	**0.9274**	0.9290	0.9165	**0.9347**

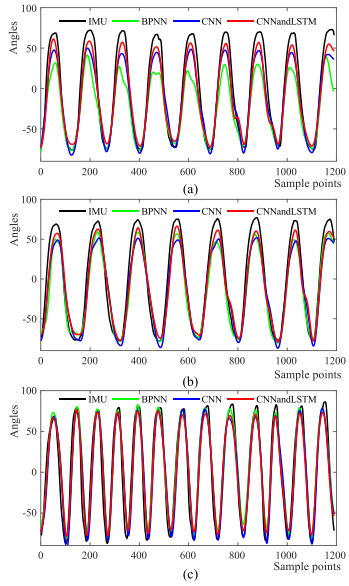

Fig. 9. Offline angle estimation results under BPNN, CNN and CNN-LSTM. (a) Angle estimation of subject 8 (b) angle estimation of subject 9 (c) angle estimation of subject 10.

TABLE IV
QUANTITATIVE EVALUATION OF ONLINE ANGLE ESTIMATION UNDER CNN-LSTM

	Estimated Angle	**Motor Angle**	
		With time delay	**Without time delay**
RMSE	10.8528	27.3740	10.6437
MAE	8.2343	23.4455	8.4758
SSE	7.0670e+04	4.4960e+05	6.7293e+04
R^2	0.9558	0.7187	0.9572

TABLE V
COMPARISON OF PREDICTION PERFORMANCE WITH OTHER METHODS

	RMSE	R^2
Yang et al. [15]	20.4400	0.8940
Zhao et al. [29]	17.5900	0.9100
Ding et al. [30]	13.2209	0.8400
This study	**15.2596**	**0.9290**

models (BPNN, CNN, CNN-LSTM) varies significantly. For Subject 9, it is evident that there is a difference in the prediction effect of the three models. But for Subject 10, there is no apparent difference in the prediction performance of the three models. Nevertheless, the quantitative indicators in Table III reveal that the CNN-LSTM model has a superior prediction effect. Whether for Subject 8, Subject 9, or Subject 10, the CNN-LSTM model has the best prediction results, demonstrating its effectiveness in addressing inter-subject variability.

2) Online Angle Estimation and Real-Time Control of GP-ULDE: Through the comparison of offline analysis, it is found that the CNN-LSTM has the best prediction effect. Therefore, the online angle estimation and real-time control of GP- ULDE are performed using the trained CNN-LSTM model. Unlike the offline phase, the online prediction and motor control phases must take into account the delay time in addition to the evaluation indicators mentioned above. Fig. 10 shows the online estimation and motor angle plotted together. The time lag between the IMU angle and the estimation angle (as well as the time lag between IMU angle and motor angle) is calculated. It can be seen from Fig. 10(a) and (d) that there exists no time lag between the IMU angle and the estimation angle. But the motor angle experiences an inevitable delay compared to the IMU angle. The time lag is calculated by a fast linear correlation algorithm. The calculation result is shown in Fig. 10(e). The phase difference between the IMU angle signal and the motor angle signal is 6 sampling points. Because the window length of sEMG is 250 ms with an increment of 50 ms, the interval between the two sequences is 300 ms ($6 \times 50 = 300$ ms). Table IV records the quantitative evaluation values for the estimation and motor angles compared to the IMU angles.

IV. DISCUSSION

In this study, a home-based upper limb rehabilitation system has been developed. In this system, the GP-ULED serves as the rehabilitation device, and sEMG-based subject-independent estimation of continuous movements is realized through the CNN-LSTM. The combination of the portable upper limb exoskeleton and Myo armband meets the requirements of home-based rehabilitation. By utilizing CNN-LSTM to extract transferable features, intention estimation of cross-subject continuous movements can be realized. The effectiveness of the system is verified through both offline and online experiments.

Table III reflects the variability among different subjects. The evaluation criteria of MAE and R^2 are taken as examples to illustrate. Under the BPNN model, MAE values of the three test subjects (8-10) are 22.7426, 14.4615, and 12.1731, respectively, and R^2 values are 0.7106, 0.8979, and 0.9290, respectively, which reflects the variability and also indicates that this model lacks generalization ability among different subjects. Under the CNN-LSTM model, MAE values of the three test subjects (8–10) are 12.8540, 13.0131, and 11.3080, respectively, and R^2 values are 0.9250, 0.9274, and 0.9347, respectively, which indicates that CNN-LSTM can extract transferable features, thus inhibiting variability and enabling the model to have generalization ability among different subjects.

The comparison results of different methods are summarized in Table V, which shows that the RMSE using the proposed

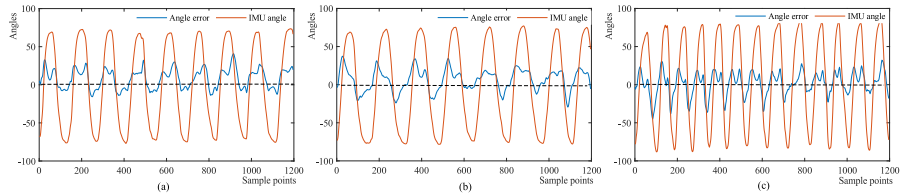

Fig. 10. Angle error distribution between the estimation angle and IMU angle. (a) Subject 8 (b) subject 9 (c) subject 10.

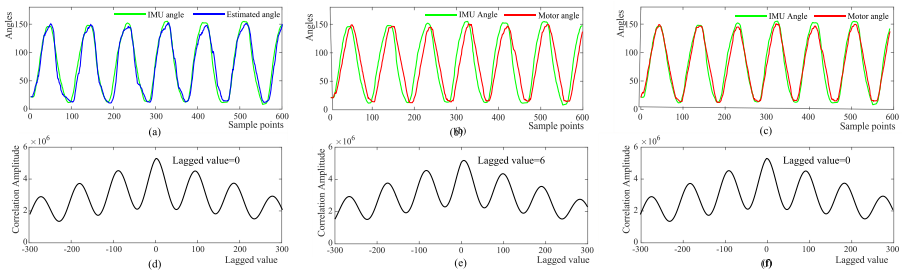

Fig. 11. Online estimation and motor angle. (a) Estimated angle (b) motor angle (c) motor angle without time lag (d) phase difference between the signal of estimated angles and IMU angles (e) phase difference between the signal of motor angles and IMU angles (f) phase difference between the signal of motor angles and IMU angles after time lag elimination.

method in this study is smaller than that reported by Yang et al. [15] and Zhao et al. [29]. Meanwhile, the R^2 of this study is greater than that of Yang et al. [15] and Zhao et al. [29]. Although the R^2 of this study is larger than that of Ding et al. [30], the RMSE of this work is smaller than that of Ding et al. [30]. The main reasons are twofold. Firstly, the modeling and testing data in the study of Ding et al. [30] are from the same subject. Secondly, the frequency of the sEMG acquisition device is much higher than that of the Myo armband used in this letter, so that more details of the sEMG signal can be collected, and better estimation can be achieved. Fig. 10 shows the distribution of errors between the estimation angles and IMU angles. It can be observed that the magnitude of the error angle is consistent with the trend of the movements, which is also an essential factor to consider for improving the prediction accuracy in the future. As shown in Fig. 11, the time delay in this study is 300 ms. It is acceptable according to [31], which recommended the maximum latency of 300 ms first.

Compared with the results of other research using robot-assisted devices to facilitate the elbow movements of flexion and extension, this research considers the requirements of home-based rehabilitation and the inter-subject variability, and few studies addressed the inter-subject variability of sEMG signal. For example, Yang et al. [15] designed an sEMG-based bilateral training system for upper limb rehabilitation in which the neural network model was established for each participant. Liu et al. [9] developed a bilateral upper limb training system for home-based rehabilitation using an sEMG-driven musculoskeletal model. Li et al. [17] implemented the sMEG-based user-independent estimation of continuous movements using the combination of multisource domain adaptation (MDA) and BPNN. The verification is currently only done offline due to the delay of the existing online MDA method, which cannot meet the real-time control requirements in HRIs.

While this research has its advantages and application potential for subject-independent home-based upper limb rehabilitation, the limitations of this study also need to be discussed. Firstly, it can be seen from Fig. 10(a) and (d) that there is no time lag between the IMU angle and the estimation angle. The sEMG signal is generally generated 30–150 ms before limb movements, which is one of the reasons for the above phenomenon. Another reason is that sliding windowing and moving average filtering can cause the current signal to exhibit the trend of future signals. But the motor angle has an inevitable delay compared to the IMU angle. Therefore, there is no delay in the prediction process, it occurs during the motor control process. Secondly, although recent studies [27], [28] have shown that deep neural networks are capable of learning transferable features, their transferability is limited. Hence, it is vital to enhance the transferability of task-specific layers. Long et al. [27] proposed a novel deep adaptation network architecture to enhance the transferability of features from task-specific layers. However, it cannot realize online learning, which means that the network requires a targeted dataset to achieve transferability. He et al. [32] proposed an online approach for cross-subject emotion recognition from ECG signals through unsupervised domain adaptation. The latency of this algorithm is 4.91 seconds, which is far from meeting the requirements of real-time control in HRIs. Thirdly, all experiments related to this study are conducted on healthy subjects, and no experiment is carried out on stroke patients.

Based on the above discussion, our future study will focus on improving the transferability of deep neural networks, such as by adding adaptive layers, and subsequently applying the updated neural network to scenarios of online estimation and real-time control. At the same time, the delay of motor control will also be considered to improve the rehabilitation system and carry out experiments for stroke patients.

V. Conclusion

In this letter, an upper limb rehabilitation system that takes into account both the portability of the exoskeleton and the inter-subject variability of sEMG is established. The upper limb exoskeleton, the offline training and comparison of estimation results, the online estimation, and real-time control of the GP-ULED are systematically introduced and analyzed. The effectiveness of the CNN-LSTM model in achieving subject-independent estimation of continuous movements has been verified, and the model is then applied to the real-time control of the upper limb rehabilitation exoskeleton.

Acknowledgment

The authors would like to acknowledge all the subjects for participating in this research.

Reference

[1] G. Poomalai, S. Prabhakar, and N. Sirala Jagadesh, "Functional ability and health problems of stroke survivors: An explorative study," *Cureus*, vol. 15, no. 1, Jan. 2023, Art. no. e33375.

[2] J. Narayan, B. Kalita, and S. K. Dwivedy, "Development of robot-based upper limb devices for rehabilitation purposes: A systematic review," *Augmented Hum. Res.*, vol. 6, no. 1, pp. 1–33, Jan. 2021.

[3] A. Cerasa et al., "Exoskeleton-robot assisted therapy in stroke patients: A lesion mapping study," *Front. Neuroinform.*, vol. 17, no. 12, Jul. 2018, Art. no. 44.

[4] J. Wu, H. Cheng, J. Zhang, Z. Bai, and S. Cai, "The modulatory effects of bilateral arm training (BAT) on the brain in stroke patients: A systematic review," *Neurological Sci.*, vol. 42, no. 2, pp. 501–511, Nov. 2021.

[5] E. Trigili et al., "Detection of movement onset using EMG signals for upper-limb exoskeletons in reaching tasks," *J. Neuroengineering Rehabil.*, vol. 16, no. 45, pp. 1–16, Mar. 2019.

[6] L. Bi, A. G. Feleke, and C. Guan, "A review on EMG-based motor intention prediction of continuous human upper limb motion for human-robot collaboration," *Biomed. Signal Process Control*, vol. 51, pp. 113–127, May 2019.

[7] Y. Zhang, Y. Chen, H. Yu, X. Yang, and W. Lu, "Learning effective spatial-temporal features for sEMG armband-based gesture recognition," *IEEE Internet Things*, vol. 7, no. 8, pp. 6979–6992, Aug. 2020.

[8] D. Buongiorno, F. Barone, M. Solazzi, V. Bevilacqua, and A. Frisoli, "A linear optimization procedure for an EMG-driven neuromusculoskeletal model parameters adjusting: Validation through a myoelectric exoskeleton control," *Haptics: Percep., Devices, Control, Appl.*, vol. 9775, pp. 218–227, Jul. 2016.

[9] Y. Liu, S. Guo, Z. Yang, H. Hirata, and T. Tamiya, "A home-based bilateral rehabilitation system with sEMG-based real-time variable stiffness," *IEEE J. Biomed. Health Inform.*, vol. 25, no. 5, pp. 1529–1541, May 2021.

[10] L. Peng, Z.-G. Hou, L. Peng, and W.-Q. Wang, "Experimental study of robot-assisted exercise training for knee rehabilitation based on a practical EMG-driven model," in *Proc. IEEE 6th Int. Conf. BioRob*, 2016, pp. 810–814.

[11] D. Ao, R. Song, and J. Gao, "Movement performance of human-robot cooperation control based on EMG-driven Hill-type and proportional models for an ankle power-assist exoskeleton robot," *IEEE Trans. Neural Syst. Rehabil. Eng.*, vol. 25, no. 8, pp. 1125–1134, Aug. 2017.

[12] H. Cai, S. Guo, Z. Yang, and J. Guo, "A motor recovery training and evaluation method for the upper limb rehabilitation robotic system," *IEEE Sensor J.*, vol. 23, no. 9, pp. 9871–9879, May 2023.

[13] Z. Yang, S. Guo, Y. Liu, M. Kawanishi, and H. Hirata, "A task performance-based sEMG-driven variable stiffness control strategy for upper limb bilateral rehabilitation system," *IEEE/ASME Trans. Mechatronics*, vol. 28, no. 2, pp. 792–803, Apr. 2023.

[14] Y. Liu, S. Guo, Z. Yang, H. Hirata, and T. Tamiya, "A home-based tele-rehabilitation system with enhanced therapist-patient remote interaction: A feasibility study," *IEEE J. Biomed. Health Inform.*, vol. 26, no. 8, pp. 4176–4186, Aug. 2022.

[15] Z. Yang, S. Guo, Y. Liu, H. Hirata, and T. Tamiya, "An intention-based online bilateral training system for upper limb motor rehabilitation," *Microsystem Technol.*, vol. 27, pp. 211–222, Jun. 2021.

[16] F. Xiao, Y. Wang, Y. Gao, Y. Zhu, and J. Zhao, "Continuous estimation of joint angle from electromyography using multiple time-delayed features and random forests," *Biomed. Signal Process.*, vol. 39, pp. 303–311, Jan. 2018.

[17] H. Li, S. Guo, H. Wang, and D. Bu, "Subject-independent continuous estimation of sEMG-based joint angles using both multisource domain adaptation and BP neural network," *IEEE Trans. Instrum. Meas.*, vol. 72, 2023, Art. no. 4000910.

[18] M. Hakonen, H. Piitulainen, and A. Visala, "Current state of digital signal processing in myoelectric interfaces and related applications," *Biomed. Signal Process.*, vol. 18, pp. 334–359, Apr. 2015.

[19] E. Trigili et al., "Detection of movement onset using EMG signals for upper-limb exoskeletons in reaching tasks," *J. Neuroengineering Rehabil.*, vol. 16, no. 1, pp. 1–16, Mar. 2019.

[20] Y. Guo, X. Gu, and G.-Z. Yang, "MCDCD: Multisource unsupervised domain adaptation for abnormal human gait detection," *IEEE J. Biomed. Health Inform.*, vol. 25, no. 10, pp. 4017–4028, Oct. 2021.

[21] C. Lambelet, M. Lyu, D. Woolley, R. Gassert, and N. Wenderoth, "The eWrist—A wearable wrist exoskeleton with sEMG-based force control for stroke rehabilitation," in *Proc. IEEE Int. Conf. Rehabil. Robot.*, 2017, pp. 726–733.

[22] Thalmic Labs, 2013. Accessed: Nov. 1, 2017. [Online]. Available: https://www.myo.com/

[23] C. Lambelet, D. Temiraliuly, M. Siegenthaler, M. Wirth, and N. Wenderoth, "Characterization and wearability evaluation of a fully portable wrist exoskeleton for unsupervised training after stroke," *J. Neuroengineering Rehabil.*, vol. 17, no. 1, pp. 1–16, Oct. 2020.

[24] M. Y. b. Yakob, M. Z. b. Baharuddin, A. R. M. Khairudin, and M. H. B. A. Karim, "Telecontrol of prosthetic robot hand using MYO armband," in *Proc. IEEE Int. Conf. Autom. Control Intell. Syst.*, 2021, pp. 288–293.

[25] M. Melero, A. Hou, E. Cheng, A. Tayade, and N. Navab, "Upbeat: Augmented reality-guided dancing for prosthetic rehabilitation of upper limb amputees," *J. Healthcare Eng.*, vol. 2019, Mar. 2019, Art. no. 2163705.

[26] E. Otović, M. Njirjak, D. Jozinović, G. Mauša, A. Michelini, and I. Štajduhar, "Intra-domain and cross-domain transfer learning for time series data—How transferable are the features?," *Knowl. Based Syst.*, vol. 239, Mar. 2022, Art. no. 107976.

[27] M. Long, Y. Cao, Z. Cao, J. Wang, and M. I. Jordan, "Transferable representation learning with deep adaptation networks," *IEEE Trans. Pattern Anal. Mach. Intell.*, vol. 41, no. 12, pp. 3071–3085, Dec. 2019.

[28] A. Agga, A. Abbou, M. Labbadi, Y. El Houm, and I. Hammou Ou Ali, "CNN-LSTM: An efficient hybrid deep learning architecture for predicting short-term photovoltaic power production," *Elect. Power Syst. Res.*, vol. 208, Jul. 2022, Art. no. 107908.

[29] Y. Zhao, Z. Zhang, Z. Li, Z. Yang, A. A. Dehghani-Sanij, and S. Xie, "An EMG-driven musculoskeletal model for estimating continuous wrist motion," *IEEE Trans. Neural Syst. Rehabil. Eng.*, vol. 28, no. 12, pp. 3113–3120, Dec. 2020.

[30] Q. Ding, G. Zhao, and J. Han, "EMG-based estimation for multi-joint continuous movement of human upper limb," *Robot*, vol. 36, no. 4, pp. 469–476, Jul. 2014.

[31] B. Hudgins, P. Parker, and R. N. Scott, "A new strategy for multifunction myoelectric control," *IEEE Trans. Biomed. Eng.*, vol. 40, no. 1, pp. 82–94, Jan. 1993.

[32] W. He, Y. Ye, Y. Li, T. Pan, and L. Lu, "Online cross-subject emotion recognition from ECG via unsupervised domain adaptation," in *Proc. IEEE 43rd Annu. Int. Conf. IEEE Eur. Mol. Biol. Conf.*, 2021, pp. 1001–1005.